well fitted by the imperfect-lattice $G^{(11)}_{T_{1u}}(\omega)$ response function with only small percentage changes in the lattice force constants. The multiphonon region can be constructed with successive coupling to the $G_{E_g}(\omega)$ response function. This could easily be understood if there were an E_g Jahn-Teller distortion in the excited state. However, there is another coupling mechanism which could explain this coupling and it has not been possible to conclusively establish the presence of such a Jahn-Teller distortion.

The crude point-charge calculation of one-phonon coupling which was used successfully for previous transitions of impurities in MgO has been used without success—placing some doubt on the validity of such a model.

ACKNOWLEDGMENTS

I would like to acknowledge the advice and encouragement of Dr. R. W. H. Stevenson, and Professor C. McCombie and Dr. M. J. Sangster for the use of their computer calculation of Green's functions. Thanks also to my colleagues for many useful discussions.

†Research conducted at University of Aberdeen supported by the Science Research Council and at UCLA supported by U. S. Army Research Office, Durham, N.C.

*Now at Queen Mary College, London, England.

[1]N. B. Manson, preceding paper, Phys. Rev. B 4, 2645 (1971).

[2]J. E. Ralph and M. G. Townsend, J. Phys. C 3, 8 (1970).

[3]J. E. Ralph and M. G. Townsend, J. Chem. Phys. 48, 149 (1968).

[4]A. D. Liehr and C. J. Ballhausen, Am. J. Phys. (N.Y.) 6, 134 (1959).

[5]H. A. Jahn and E. Teller, Proc. Phys. Soc. (London) A161, 220 (1937).

[6]M. D. Sturge suggested for similar transition in MgO: Ni^{2+} in Ref. 7, p. 184.

[7]M. D. Sturge, in *Solid State Physics*, edited by F. Seitz and D. Turnbull (Academic, New York, 1967), Vol. 20, p. 91.

[8]M. J. L. Sangster and C. W. McCombie, J. Phys. C 3, 1498 (1970).

PHYSICAL REVIEW B VOLUME 4, NUMBER 8 15 OCTOBER 1971

Vibronic Structure and Optical Properties of the $M(C_{2h})$ Center in MgF_2 †

M. Mostoller, B. Henderson,* W. A. Sibley,‡ and R. F. Wood
Solid State Division, Oak Ridge National Laboratory, Oak Ridge, Tennessee 37830
(Received 10 March 1971)

The optical properties of the $M(C_{2h})$ center in MgF_2 are analyzed in terms of an effective one-phonon density of states, using a combination of convolution integration and moment analysis. A satisfactory fit to the experimental absorption spectrum at $T=0$ is obtained for this intermediate coupling case, including particularly the sharp structure seen in the one-phonon region. Good agreement between theory and experiment is also found for the no-phonon line and broad-band parameters in absorption as functions of temperature. A calculated luminescence spectrum, derived from that for absorption by using a simple model to estimate the quadratic coupling, compares well with the observed emission band at $T=0$.

I. INTRODUCTION

A practical procedure for calculating the optical absorption and emission spectra of impurities in insulators was described in a recent paper by Mostoller, Ganguly, and Wood[1] (referred to hereafter as MGW). The computational approach was based on the well-known theory of optical processes associated with such impurities. It provided for (i) an iterative scheme for finding an effective one-phonon density of states; (ii) the convolution of this one-phonon spectrum to find the contributions of the n-phonon processes in those regions where vibronic structure occurs; (iii) the use of moment analysis for higher n-phonon processes which do not contribute discernible structure; (iv) the retention of the lowest-order effects of quadratic coupling on the temperature dependence of the zero-phonon line's half-width and peak position; (v) a simple transformation between phonon operators in the ground and excited electronic states of the impurity which breaks the mirror symmetry between the absorption and emission spectra characteristic of the linear coupling approximation. As an illustrative example, the absorption spectrum of the N_1 center in NaCl was chosen because it exhibits a great deal of phonon structure. However, little is known about either its emission spectrum (if it exists) or the temperature dependence of its zero-phonon line, so that some aspects of the computational approach could not be tested.

In this paper the results of a combined experimental and theoretical study of one of the M centers in MgF_2 are presented.[2,3] An M center consists of two F centers (an electron in a negative-ion vacancy) immediately adjacent to each other in the lattice. In the rutile structure of MgF_2 there are four different M-center configurations, each with its own symmetry which can be determined from studies of the anisotropic absorption of the observed bands. One of these configurations has C_{2h} symmetry, and absorption and emission bands peaking at about 3.35 and 2.96 eV, respectively. The zero-phonon line associated with the electronic transition producing the bands is visible, and other vibronic structure is readily observed in absorption. With care, remnants of this structure can also be detected in emission. Thus, for a number of reasons, this is an interesting defect on which to test the theory. However, it does have the drawback that absorption and emission bands due to other centers are known to occur in the same spectral region, and the extraction of such underlying bands is difficult to carry out entirely unambiguously.

Although considerable experimental data about this center have already been published,[3] more extensive and refined data were collected in order to provide a better basis for comparison with theoretical results. The experimental procedure is described briefly in Sec. II, and the most important equations employed in the theoretical analysis are listed in Sec. III. The calculated results and their comparison with experiment are presented in Sec. IV. A brief discussion of the relationship between the one-configurational-coordinate model and the more general approach employed here is given in Sec. V.

II. EXPERIMENTAL PROCEDURE

As in previously reported work,[3] single-crystal ingots of MgF_2 were cut into samples 0.5–1.0 mm thick, oriented so that their optical faces were parallel to the c axis. The crystals were irradiated with 2.0-MeV electrons and bleached with 254-nm light at room temperature to produce and enhance the $M(C_{2h})$ bands. Optical absorption and emission measurements were made with the samples mounted in a cryostat, with temperatures measured by a Pt-resistance thermometer.

In absorption, the no-phonon line and the structure in the one-phonon region were measured with a Jarrell-Ash monochromator, having a linear dispersion of 8 A/mm and slit widths of 5–50 μ, in conjunction with a cooled 9558 multiplier phototube. This detection system was calibrated with a standard quartz-iodine lamp. For optical densities greater than unity, which for the crystals studied meant for photon frequencies more than about 0.035 eV above the no-phonon line, the Jarrell-Ash system was less accurate than the Cary 14R double-beam spectrophotometer previously used for the entire absorption band. Therefore, data were taken on both systems and normalized at the first one-phonon peak, which is broad enough to make instrumental broadening by the Cary 14R unimportant. With the normalization process included, the absorption measurements were reproducible to within the order of 10% or less.

Luminescence was excited by a mercury lamp mounted to a $\frac{1}{2}$-m Bausch and Lomb monochromator, and the spectrum was measured with the Jarrell-Ash system. The vibronic structure is weaker in intensity and thus experimental uncertainties are considerably larger in emission than in absorption for this center. We will therefore focus somewhat more on absorption than emission in what follows. All experimental data will be shown later when comparisons with the calculations are made.

III. THEORETICAL MODEL AND CALCULATIONAL PROCEDURES

Since the theoretical approach has been described in detail in MGW, only a brief summary of the necessary equations and calculational procedures will be given here. Optical absorption and emission due to transitions between the ground electronic state a and a nondegenerate excited state b of an interacting defect-lattice system are treated within the framework of the adiabatic and Condon approximations, under the assumption that the phonons are in internal thermal equilibrium. The cross section for photon absorption $\sigma_{ab}(\omega)$, and the spontaneous emission probability $W_{ba}(\omega)$, can then be written as

$$\sigma_{ab}(\omega) = K_{\rm abs} \mid M_{ab} \mid^2 \omega G(ab;\ \omega) \tag{1}$$

and

$$W_{ba}(\omega) = K_{\rm em} \mid M_{ab} \mid^2 \omega^3 G(ba;\ \omega)\ , \tag{2}$$

where ω is the photon frequency, M_{ab} is the electronic dipole moment matrix element, and $K_{\rm abs}$ and $K_{\rm em}$ are essentially constants which involve the effective field ratio and the index of refraction.

The spectral function for absorption, $G(ab;\ \omega)$, is defined by

$$G(ab;\ \omega) = \int_{-\infty}^{\infty} dt\, e^{i\omega t}\, G(ab;\ t)$$

$$= \int_{-\infty}^{\infty} dt\, e^{i\omega t} \langle e^{iH_a t/\hbar} e^{-iH_b t/\hbar} \rangle_a\ , \tag{3}$$

where H_a and H_b are the ground- and excited-state phonon Hamiltonians, and $\langle\ \rangle_a$ denotes the average over the ground-state phonon ensemble. For absorption, it is convenient to write H_a and H_b in the forms

$$H_a = E_a + \sum_k \hbar\omega_k (a_k^\dagger a_k + \tfrac{1}{2}) \tag{4a}$$

and

$$H_b = H_a + \hbar\omega_{ba} + \sum_k (v_k a_k + v_k^* a_k^\dagger) + \tfrac{1}{2} \sum_{kk'} v_{kk'} (a_k + a_k^\dagger)(a_{k'} + a_{k'}^\dagger) . \tag{4b}$$

Here $a_k^\dagger$ and a_k are creation and destruction operators for phonons of mode k, while v_k and $v_{kk'}$ are linear and quadratic coupling coefficients for absorption. $\hbar\omega_{ba}$ is a static energy difference which would reduce to the purely electronic transition energy in the absence of electron-phonon coupling. For emission, when the initial state is the electronic excited state, a and b should be interchanged in Eqs. (4a) and (4b), and ω_k, a_k, $a_k^\dagger$, ω_{ba}, v_k, and $v_{kk'}$ replaced by Ω_k, A_k, $A_k^\dagger$, Ω_{ba}, V_k, and $V_{kk'}$, with the latter quantities related to the former by a linear transformation of the phonon operators. We neglect the mode-mixing terms in Eq. (4b) in order to actually perform the transformation. That is, we take $v_{kk'} = V_{kk'} = 0$ for $k \neq k'$ to find the following relationships between absorption and emission parameters:

$$\Omega_k = \gamma_k \omega_k ; \quad V_k = v_k/\gamma_k^{5/2} ; \quad V_{kk} = v_{kk}/\gamma_k , \tag{5}$$

with

$$\gamma_k = [1 + 2(v_{kk}/\hbar\omega_k)]^{1/2} . \tag{6}$$

The absorption function $G(ab;\omega)$ is found by substituting Eqs. (4a) and (4b) in Eqs. (3), performing the average, and integrating over time. Further simplifications are then made to obtain results which essentially depend only on the phonon frequencies ω_k and individual mode Huang-Rhys factors S_k,

$$S_k = |v_k|^2/(\hbar\omega_k)^2 . \tag{7}$$

The no-phonon contribution to $G(ab;\omega)$ is separated out, only the lowest-order quadratic coupling terms which give rise to the temperature dependence of its peak position and half-width are retained, and a slight generalization of the approximation $v_{kk'} = \alpha v_k v_{k'}$ is used. The no-phonon line then is a Lorentzian whose peak frequency ω_0 and half-width Γ_0 are given by

$$\hbar\omega_0(T) = \hbar\omega_{ba} - \sum_k \hbar\omega_k S_k + (\alpha_1/2\hbar\omega_D) \sum_k (\hbar\omega_k)^2 S_k [2n(\omega_k) + 1] \tag{8}$$

and

$$\hbar\Gamma_0(T) - \hbar\Gamma_0(0) = \pi(\alpha_2/\hbar\omega_D)^2 \sum_{kk'} [(\hbar\omega_k)^2 S_k] \times [(\hbar\omega_{k'})^2 S_{k'}] \, n(\omega_k)[n(\omega_k)+1] \, \delta(\hbar\omega_k - \hbar\omega_{k'}) . \tag{9}$$

Here α_1 and α_2 are adjustable parameters, ω_D is an arbitrary frequency introduced for scaling purposes, and $n(\omega_k) = [\exp(\beta\hbar\omega_k) - 1]^{-1}$.

We define the broad-band spectrum $G_B(ab;\omega)$ as the total spectrum minus the zero-phonon contribution. Except insofar as quadratic coupling is implicitly included in the linear coupling coefficients [cf. Eqs. (5) and (6)], $G_B(ab;\omega)$ is calculated in the linear coupling approximation. At $T = 0\,^\circ$K, we find that

$$G_B(ab;\omega) = \sum_{n=1}^{\infty} G_n(ab;\omega) , \tag{10}$$

with the n-phonon spectrum given by

$$G_n(ab;\omega) = e^{-S} \int_{-\infty}^{\infty} dt \exp[i(\omega - \omega_0)t] [g_1(t)]^n/n! , \tag{11}$$

where

$$g_1(t) = \sum_k S_k e^{-i\omega_k t} . \tag{12}$$

Substituting Eqs. (12) into Eq. (11), we can write the n-phonon contribution to the total spectrum as an n-fold convolution of the one-phonon spectrum, $G_1(ab;\omega)$, where, with $S = \sum S_k$,

$$G_1(ab;\omega) = 2\pi e^{-S} \sum_k S_k \delta[(\omega - \omega_0) - \omega_k] . \tag{13}$$

Moment analysis is used to determine the higher n-phonon spectra at $T = 0$, direct evaluation of convolution integrals being required only for those lower values of n for which structure is present in $G_n(ab;\omega)$. Moment analysis is also used to find the temperature dependence of the broad-band half-width.

The starting point for the application of the theory is a preliminary estimate of the one-phonon spectrum. This initial estimate need not be particularly accurate, since the iterative procedure described in MGW provides a straightforward way to obtain a refined one-phonon spectrum which yields satisfactory agreement with experiment. In the present work, as in MGW, $G_1(ab;\omega)$ is represented by a series of many evenly spaced δ-function spikes,

$$G_1(ab;\omega) = 2\pi e^{-S} \sum_k S_k \delta((\omega - \omega_0) - k\Delta) . \tag{14}$$

A width and shape could be given to these spikes, but there seems to be little point in doing so since the computer programs are capable of handling a very large number of spikes. Our curves for $G_n(ab;\omega)$ rigorously satisfy the sum rule

$$\int_{-\infty}^{\infty} d\omega \, G_n(ab;\omega) / \int_{-\infty}^{\infty} d\omega \, G_B(ab;\omega)$$

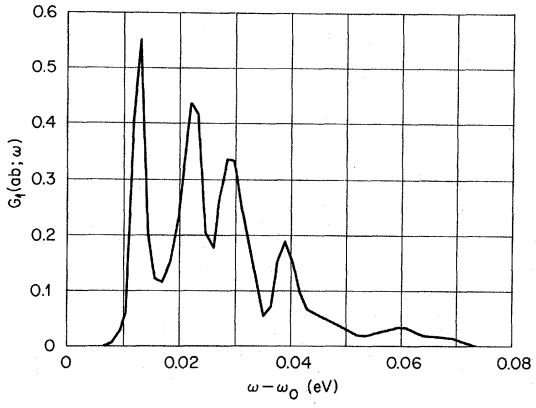

FIG. 1. The one-phonon spectrum for absorption, $G_1(ab;\omega)$. The spectrum shown has 51 peaks, with $\Delta = 0.0013$ eV and $S = \sum_k S_k = 6.257$, which fixes the ordinate scale of the plot.

$$= (S^n/n!)e^{-S}/(1-e^{-S}) . \tag{15}$$

Before going on to discuss our results for the $M(C_{2h})$ center in MgF_2, we would like to note several points. First, to obtain equations appropriate for the calculation of the broad-band spectrum in emission rather than absorption, we need only change the sign of the photon frequency relative to the no-phonon peak position and replace ω_k and S_k by Ω_k and $\mathcal{S}_k$, where, from Eqs. (5) and (7),

$$\mathcal{S}_k = S_k/\gamma_k^7 . \tag{16}$$

Also, we would like to emphasize the utility of moment analysis and the insensitivity of the iterative procedure to its starting point. Our starting one-phonon spectrum for the $M(C_{2h})$ absorption spectrum was one obtained by moment analysis; it contained no structure, but it was constructed to yield approximately correct values for the broad-band peak position and half-width. The first iteration introduced considerable structure, and succeeding steps led to the result shown in Fig. 1.

IV. THEORETICAL RESULTS AND COMPARISON WITH EXPERIMENT

Figure 1 shows the one-phonon spectrum obtained by the iterative procedure for the 3.35-eV $M(C_{2h})$ absorption band in MgF_2. It contains 51 peaks, with an interpeak spacing $\Delta = 0.0013$ eV and a total Huang-Rhys factor $S = 6.257$. The calculated n-phonon and total broad-band spectra are plotted in Fig. 2. It can be seen here how structure washes out as more convolutions are performed; moment analysis gives satisfactory results for $G_n(ab;\omega)$ for $n \geq 6$. The figure also illustrates that it is not just the one-phonon spectrum which contributes structure to the curve, since some of the humps in the total results from two- and three-phonon processes.

Figure 3 compares the calculated broad-band spectrum at $T = 0$ with the corresponding "skewed Gaussian" curve produced by moment analysis. The two differ in the low-frequency region where structure appears, and they diverge at the highest frequencies plotted, because the "exact" calculated curve omits the n-phonon contributions from $n = 13$ on up. The half-widths, however, agree to within less than $\frac{1}{2}\%$, and the peak positions to within one spacing Δ or less than 1%.

Figure 4 compares the calculated and experimental broad-band absorption spectra at $T = 0$ over the entire frequency range of the band. On the scale of the figure, agreement is particularly good in the initial region of sharp structure and in the upper-frequency half of the spectrum, and is within experimental uncertainty over the entire range. Although it is within experimental error, the discrepancy between the two curves to the left of the broad-band peak may reflect the presence

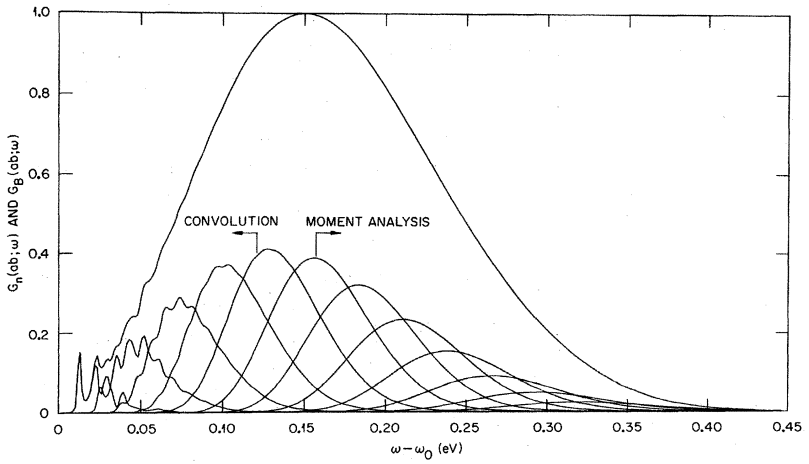

FIG. 2. The calculated broad-band spectrum for absorption and its n-phonon components at $T = 0$. $G_n(ab;\omega)$ was found by convoluting the one-phonon spectrum for $n = 1$–5 and by moment analysis for $n = 6$–12.

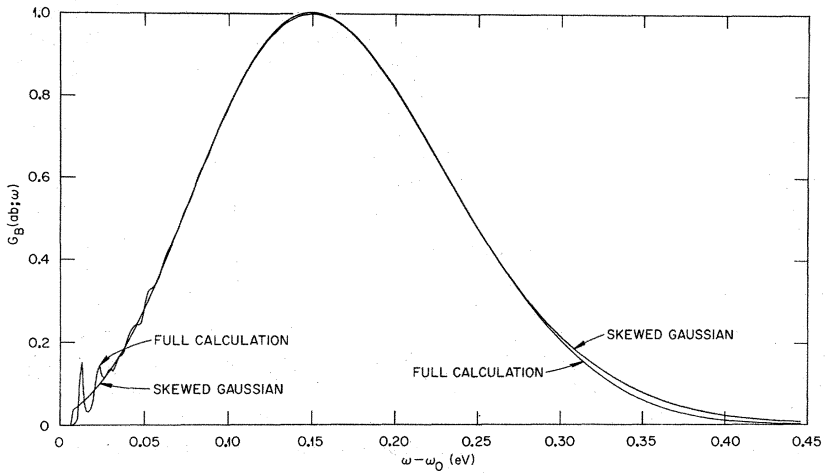

FIG. 3. The calculated total broad-band curve in Fig. 2 compared with the corresponding skewed Gaussian curve obtained by moment analysis.

of another, relatively weak, absorption band or bands in this region. The normalization procedure used to fit the data taken on the Jarrell-Ash monochromator to those taken on the Cary 14R instrument may also be responsible for some of the discrepancy. Weak structure has been reported[3] above the frequency range of the Jarrell-Ash spectrophotometer, but because of the relatively poor resolution possible, no attempt was made to include this in the composite experimental plot. However, two rather pronounced humps do appear above 0.040 and 0.050 eV in the calculated spectrum, which is about where these humps are seen experimentally.

Figure 5 compares the calculated and experimental spectra in the region of best experimental resolution, including also the one-phonon contribution to the theoretical envelope. Table I lists calculated and experimental values for the absorption strengths at the peaks and valleys seen in Fig. 5, and for the broad-band peak frequency and half-width at $T=0$. The calculated curve tracks the experimental spectrum from above, with point-by-point comparison showing agreement to within 10–15%; in terms of the height at the broad-band maximum, the differences are only of the order of 1–2% or less in magnitude. The process by which the one-phonon spectrum is determined is well illustrated in Fig. 5 by the dip occurring at 0.026 eV. A substantial two-phonon peak appears at about this frequency because of the strong one-phonon peak at 0.013 eV, so in order to obtain the slight dip observed in the total spectrum at 0.026 eV, a rather deep valley is required in the one-phonon spectrum.

For the $M(C_{2h})$ center, emission data could not be obtained with the same accuracy as for absorption and hence our comparison of theory and experiment cannot be as detailed as it was for absorption. For this reason, we use a very simple model

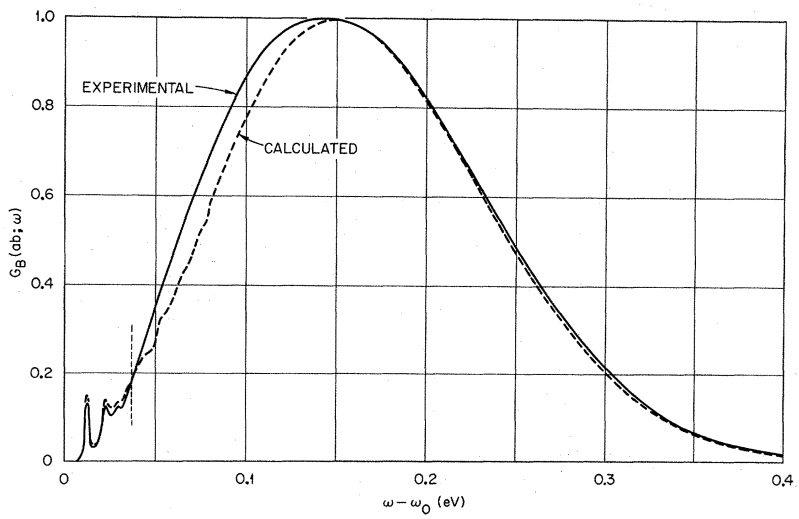

FIG. 4. Calculated and experimental results for $G_B(ab;\omega)$ at $T=0$.

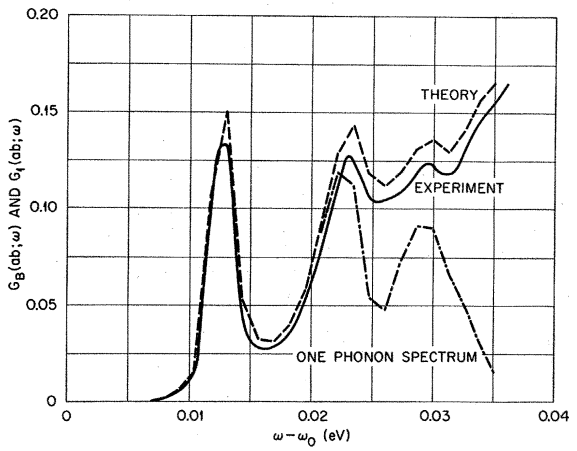

FIG. 5. Calculated and experimental results for $G_B(ab;\omega)$ at $T=0$ in the frequency range of best experimental resolution. The one-phonon contribution to the theoretical curve is also shown.

for the quadratic coupling and attempt only to fit the broad-band peak position and half-width in emission at $T=0$. Keeping only the diagonal quadratic coupling as described in Sec. III, we make the further approximation that

$$v_{kk}=\epsilon\hbar\omega_k\,, \tag{17}$$

where ϵ is a constant. From Eqs. (5) and (16), the phonon frequencies and Huang-Rhys factors for emission are then related to those in absorption by

$$\Omega_k=\gamma_0\omega_k\,,\quad S_k=S_k/\gamma_0^7\,, \tag{18}$$

with

$$\gamma_0=(1+2\epsilon)^{1/2}\,. \tag{19}$$

Figure 6 shows the calculated broad-band absorption and emission functions $G_B(ab;\omega)$ and $G_B(ba;\omega)$ obtained with the value $\gamma_0=0.922$, which yields a total Huang-Rhys factor of 11.047 in emission. Compared with that for absorption, the emission spectrum is noticeably broader and peaked further from the no-phonon line, and structure is suppressed by the higher Huang-Rhys factor so that it is just barely visible. The calculated broad-band peak position in emission (referred to the no-phonon line) is -0.251 eV and the half-width 0.210 eV, which compare well with the experimental values of -0.238 and 0.216 eV, respectively. The lowest two, essentially one-phonon, peaks in emission fall at $\omega-\omega_0=-0.012$ eV and $\omega-\omega_0\simeq-0.023$ eV, while the experimental values are -0.013 and -0.026 eV. Given the extreme simplicity of the theoretical approach and the experimental uncertainties, this is quite good agreement.

TABLE I. MgF_2 M-center absorption at $T=0$: broad-band peak position and half-width, and values for $G_B(ab;\omega)$ at the three peaks and valleys observed in the frequency range of best resolution.

	Calc	Expt	Discrepancy (%)
$\omega_{max}-\omega_0$, eV	0.151	0.143	6
$\Delta\omega$, eV	0.174	0.186	6
1st peak	0.151	0.133	14
1st valley	0.032	0.028	14
2nd peak	0.139	0.127	9
2nd valley	0.116	0.104	11
3rd peak	0.134	0.123	9
3rd valley	0.130	0.118	10

Figure 7 compares calculated and experimental results for the broad-band half-width as a function of temperature in absorption $[\omega G_B(ab;\omega)]$ and emission $[\omega^3 G_B(ba;\omega)]$. In order to minimize the possible effects of other bands, the function plotted is $\Delta\omega(T)-\Delta\omega(0)$. For absorption, the agreement is good. For emission, however, the experimental points rise more rapidly with increasing temperature than the calculated curve. To the extent that this discrepancy cannot be accounted for by experi-

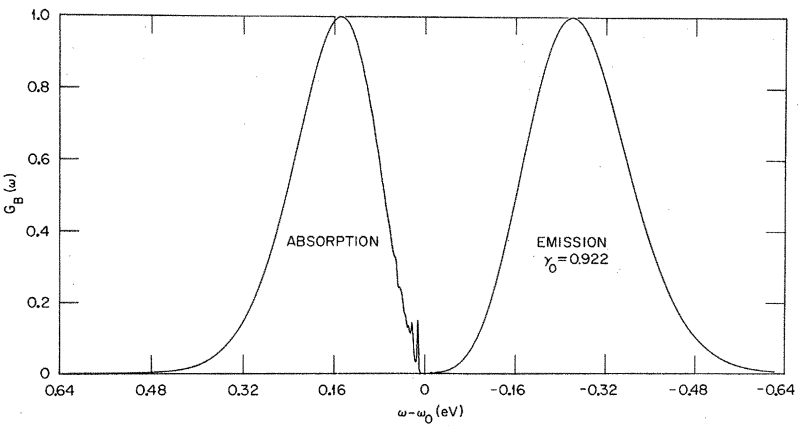

FIG. 6. Calculated absorption and emission at $T=0$.

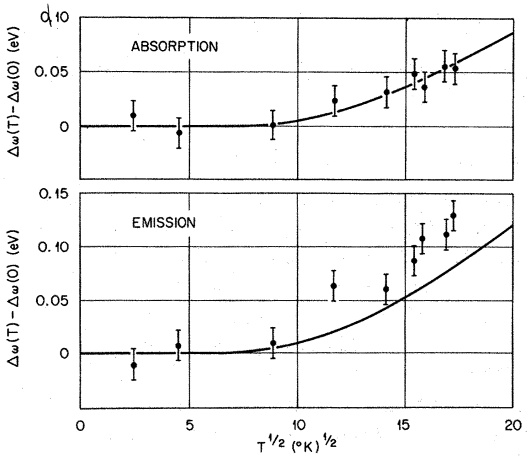

FIG. 7. Broad-band half-width in emission and absorption as a function of temperature.

mental uncertainty or the possibility of other temperature-dependent emission bands in the same frequency region, it suggests that we have not weighted the low-frequency part of the one-phonon spectrum for emission enough with our simple model for the diagonal quadratic coupling.

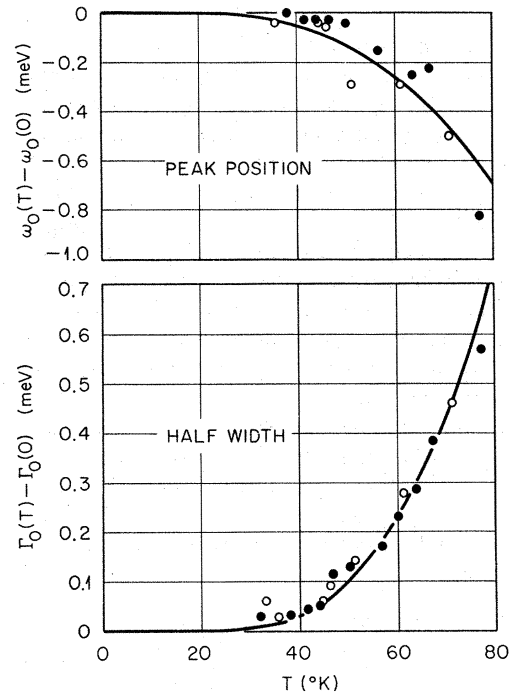

FIG. 8. The no-phonon-line peak position and half-width as functions of temperature. The open and closed circles are experimental points taken in two different runs on the same crystal. The parameters used to obtain the calculated curves are $\alpha_1 = 0.174$, $\alpha_2 = 3.43$, and $\omega_D = \sum_k \omega_k S_k / \sum_k S_k = 0.0272$ eV.

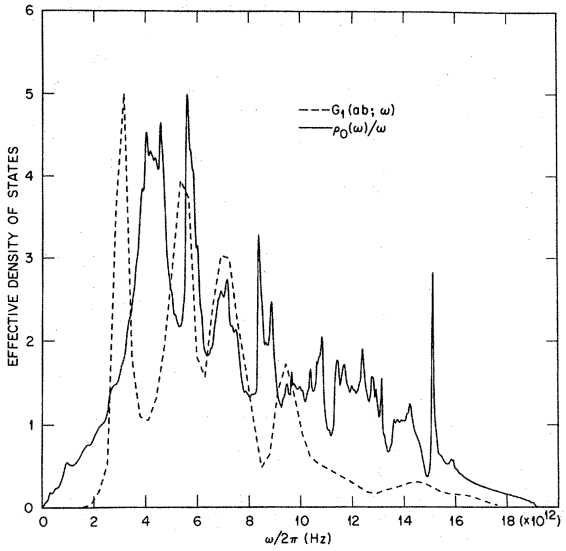

FIG. 9. A comparison of $G_1(ab;\omega)$ with the perfect lattice function $\rho_0(\omega)/\omega$.

Figure 8 shows the temperature dependence of the no-phonon line peak position ω_0 and half-width Γ_0 in absorption. As can be seen, the experimental scatter is large, and it may be recalled that the theoretical treatment of the no-phonon line is more involved than that of the broad-band spectrum. For these reasons, the no-phonon line was not used for fitting purposes. The one-phonon spectrum shown in Fig. 1 was obtained without reference to no-phonon-line data, and the calculated curves in Fig. 8 were found simply by substituting that spectrum into Eqs. (8) and (9) and varying α_1 and α_2, making the additional assumption that the temperature dependence of ω_{ba} in Eq. (8) is negligible. The results are in adequate agreement with experiment.

Finally, Fig. 9 compares the one-phonon spectrum for absorption $G_1(ab;\omega)$ with the perfect lattice density of states function $\rho_0(\omega)/\omega$. The latter was calculated[4] by the linear interpolation method of Gilat and Raubenheimer,[5] using an axially symmetric rigid-ion model for the lattice dynamics with force constants taken from Katiyar.[6] There is rather little experimental data available on the phonon dispersion curves of MgF_2, and the axially symmetric rigid-ion model is probably inadequate to fit all branches of the spectrum, so we might expect the calculation to give only the gross features of $\rho_0(\omega)/\omega$ correctly. In fact, the two curves in Fig. 9 span the same frequency range, and the four major peaks in $G_1(ab;\omega)$ correspond rather well to structure seen in $\rho_0(\omega)/\omega$.

V. DISCUSSION

We have obtained generally good agreement with

TABLE II. Various one-configurational-coordinate fits to experimental broad-band data. All frequencies are in eV, with the peak frequencies given relative to the no-phonon line. Experimental values are marked with asterisks.

Absorption	Eqs. (20), (21)	Eqs. (20), (22)	Eqs. (21), (22)
ω_g	0.0437	0.0351[a]	0.0351[a]
S_g	3.28	4.07	5.06
$\omega_{max}(0)$	0.143*	0.143*	0.178
$\Delta\omega(0)$	0.186*	0.167	0.186*
Emission			
ω_e	0.0354	0.0223[a]	0.0223[a]
S_e	6.73	10.67	16.92
$\omega_{max}(0)$	−0.238*	−0.238*	−0.377
$\Delta\omega(0)$	0.216*	0.172	0.216*

[a]Reference 3.

the experimental results for the optical spectra of the $M(C_{2h})$ center in MgF_2 by using the approach outlined in Sec. II. An essential input for our iterative calculation of the effective one-phonon density of states was the sharp vibronic structure which is well resolved in absorption. Since this structure occurs in the tails of Gaussian-like broad-band curves of the kind often treated by a one-configurational-coordinate model, it is instructive to look at the results of this simpler treatment. The obvious disadvantage of the one-configurational-coordinate model here is that it cannot reproduce the vibronic structure, and that it can only provide a limited amount of information about the average electron-phonon coupling. However, we will also find that in the present case it does not give a very good fit to gross broad-band properties, at least in its simplest form, and that it therefore yields only rough estimates of average phonon frequencies and Huang-Rhys factors.

As shown in MGW, the standard one-configurational-coordinate equations may be derived from the more general results by reducing the number of phonon modes to one and assuming that non-Gaussian corrections to the broad-band peak position and half-width are negligible. Denoting the single-mode frequency and Huang-Rhys factor for absorption by ω_g and S_g, we find that the broad-band peak position (referred to the no-phonon line) and half-width at $T=0$ in absorption are

$$\omega_{max}(0) = \omega_g S_g \tag{20}$$

and

$$\Delta\omega(0) = (8\ln 2)^{1/2}\,\omega_g S_g^{1/2}\,, \tag{21}$$

while the variation of the half-width with temperature is given by

$$\Delta\omega(T)/\Delta\omega(0) = [\coth(\beta\hbar\omega_g)\,]^{1/2}\,. \tag{22}$$

Emission parameters ω_e and S_e are defined in the same way. Equations (20)–(22) provide three equations for two unknowns, and thus overdetermine ω_g and S_g (or ω_e and S_e). For the $M(C_{2h})$ center in MgF_2, Table II shows that the ω_g, S_g and ω_e, S_e assignments from different pairs of equations are quite different. The frequencies differ by 24 and 59% in absorption and emission, respectively, while the Huang-Rhys factors have ranges of 54 and 152%. An alternative statement of the same point is that if ω_g, S_g or ω_e, S_e are found from any pair of equations, the third yields results which do not agree well with experiment. This is also shown in Table II. The total Huang-Rhys factor can also be estimated from the ratio of the integrated intensity of the no-phonon line to the total intensity [cf. Eq. (15)]. The values obtained in this way by Facey and Sibley[3] were $S_g = 4.7$ and $S_e = 8.0$. Unfortunately, although the relative intensity of the no-phonon line does fix the Huang-Rhys factor in principle, it is usually quite difficult to make anything but a rough estimate from experiment.

Thus, we see that in the present example a simple one-configurational-coordinate model provides only broad limits for a few average parameters without yielding any vibronic structure. This is not surprising, and should not obscure the usefulness of rough one-configurational-coordinate estimates of the parameters needed for the more general approach we have used. Simple configurational-coordinate models can be viewed as a kind of shorthand for moment analysis and their utility in applications to color centers is well known. In their study of the F center in KCl, for example, Klick, Patterson, and Knox[7] used a semiclassical model which included quadratic coupling and found that they could obtain a good fit to the absorption spectrum. However, the limitations of this model show up in this case also, since the emission spectrum could not be predicted with the absorption parameters.

ACKNOWLEDGMENT

We wish to thank B. N. Ganguly for several useful discussions.

†Research sponsored by the U. S. Atomic Energy Commission under contract with Union Carbide Corporation.

*Present address: Physics Department, Keele University, Staffordshire, England.

‡Present address: Physics Department, Oklahoma

State University, Stillwater, Okla. 74074.

[1]M. Mostoller, B. N. Ganguly, and R. F. Wood, Phys. Rev. B 4, 2015 (1971). An extensive list of references is contained in this paper.

[2]R. F. Blunt and M. I. Cohen, Phys. Rev. 153, 1031 (1967).

[3]O. E. Facey and W. A. Sibley, Phys. Rev. 186, 926 (1969); Phys. Rev. B 2, 1111 (1970).

[4]M. Mostoller, J. Phys. Chem. Solids (to be published).

[5]G. Gilat and L. J. Raubenheimer, Phys. Rev. 144, 390 (1966); L. J. Raubenheimer and G. Gilat, *ibid.* 157, 586 (1967).

[6]R. S. Katiyar, J. Phys. C 3, 1693 (1970).

[7]C. C. Klick, D. A. Patterson, and R. S. Knox, Phys. Rev. 133, A1717 (1964).

PHYSICAL REVIEW B VOLUME 4, NUMBER 8 15 OCTOBER 1971

Structure in the Neutron Scattering Spectra of Zirconium Hydride†

J. G. Couch*
Southern Oregon College, Ashland, Oregon 97520

and

O. K. Harling and Lavern C. Clune
Battelle Memorial Institute, Pacific Northwest Laboratory, Richland, Washington 99352

(Received 7 June 1971)

Neutron double-differential cross sections of four polycrystalline samples of ZrH_x with hydrogen-to-zirconium ratios (x) of 0.54, 1.03, 1.56, and 2.00 have been measured with high-energy resolution by downscattering of neutrons from initial energies of 171.5 and 244.8 meV. Clear evidence of structure in the one-phonon optical peak of ZrH_2 is observed for the first time. This structure consists of two maxima located at energy transfers of 137 and 143 meV and a shoulder located at 154 meV. Similar structure is indicated for the other hydride samples but it becomes less well defined as the hydrogen-to-zirconium ratio decreases. The observed structure is compared with predictions of a central-force model calculation by Slaggie, which includes the effects of interactions between hydrogen atoms. The widths of the hydrogen vibration peaks are found to depend upon the zirconium-to-hydrogen ratio as well as upon the momentum transferred in the scattering process.

I. INTRODUCTION

One reason zirconium hydride has attracted interest during the past few years is because the hydrogen atoms appear to behave somewhat as independent Einstein oscillators in the zirconium lattice. Neutron-scattering experiments[1-5] and heat-capactiy measurements[6,7] lend support to this simple model; both give consistent results indicating a vibration-level spacing of about 140 meV. Significant differences between experiment and the Einstein model do exist, however, and they have stimulated further efforts to understand the zirconium-hydrogen system in more detail. For one thing, the widths of the optical peaks obtained by neutron-scattering experiments indicate a much broader frequency distribution than that predicted by this theoretical single-frequency model, even with Doppler broadening and contributions from low-energy acoustic modes taken into account.[8,9]

At least two models—the Gaussian-plus-Debye (GD) model[9-11] and the central-force (CF) model[12]—have been used to account for the width of the first optical peak in ZrH_2. The GD phenomenological model uses a combination of an optical level with a Gaussian distribution of frequencies plus a Debye spectrum. The CF model extends the Einstein model by taking into account the longer-range forces, the H-H interactions in particular, in explaining the broad optical peak. An interesting feature of the CF model is its prediction of structure in the optical peak.

The various published zirconium-hydride neutron double-differential cross-section results[1-5] are generally consistent with an optical-peak location and width corresponding to the first vibration level of 140 meV and ~26 meV, respectively. However, none of these data reported in the literature reveal detailed shape or structure in the optical peaks. Although previous measurements have shown that the peak shape, particularly the width, does not change significantly with hydrogen concentration,[2,7,10,11,13,14] one might expect that any finer structural characteristics of the scattering peaks will differ noticeably for different H/Zr ratios.

In the present work we report high-resolution neutron-downscattering measurements of polycrystalline zirconium hydride, carried out at two different incident energies (171.5 and 244.8 meV) and four different hydrogen concentrations ($ZrH_{0.54}$,